LEGIBILITY NOTICE

A major purpose of the Technical Information Center is to provide the broadest dissemination possible of information contained in DOE's Research and Development Reports to business, industry, the academic community, and federal, state and local governments.

Although a small portion of this report is not reproducible, it is being made available to expedite the availability of information on the research discussed herein.

LA-UR -83-796

CONF-830223--3

LA-UR--83-796

DE83 010086

TITLE: A STEREO, CYLINDRICAL DRIFT CHAMBER FOR MUON DECAY EXPERIMENTS AT LAMPF

AUTHOR(S): R. D. Bolton, R. D. Carlini, M. D. Cooper, J. S. Frank, V. E. Hart, H. S. Matis, R. E. Mischke, V. D. Sandberg, and U. Sennhauser

SUBMITTED TO: The Wire Chamber Conference-Vienna, Austria
February 15-18, 1983

DISCLAIMER

Los Alamos National Laboratory
Los Alamos, New Mexico 87545

FORM NO. 836 R4
ST. NO. 2629 5/81

MASTER

A STEREO, CYLINDRICAL DRIFT CHAMBER FOR MUON DECAY EXPERIMENTS AT LAMPF

R. D. Bolton, R. D. Carlini, M. D. Cooper, J. S. Frank, V. Hart
H. S. Matis, R. E. Mischke, V. D. Sandberg, U. Sennhauser

Los Alamos National Laboratory*,
Los Alamos, New Mexico 87545, U.S.A.

ABSTRACT: A stereo, cylindrical drift chamber has been built for use in a search for rare decay modes of the muon at LAMPF. This chamber (part of the Crystal Box detector) has 728 cells on 8 concentric annuli at alternating angles of 10° to 16° from the chamber axis and with radii from 105 to 220 mm. The basic cell cross section is (9×10) mm^2 and the inter-layer spacing is 4.7 mm. Preliminary results show the single-wire efficiencies to be greater than 99%. Based on results obtained from prototype chambers, we hope to achieve 170-μm resolution (including multiple scattering) when TDC offsets and sense-wire locations found in a careful inspection of the endplates are added to the track-finding algorithm.

*Work supported by the U.S. Department of Energy.

1. Introduction

In this paper, we report on the design, construction, and preliminary testing of a stereo, cylindrical drift-chamber[1] that will be used in a search for rare decay modes of the muon[2] at the Clinton P. Anderson Meson Physics Facility (LAMPF). This experiment will search for the decays $\mu \to e\gamma$, $\mu \to e\gamma\gamma$, and $\mu \to eee$ with a sensitivity to branching ratios as low as 10^{-11}. To reach this sensitivity, a new detector system called the "Crystal Box" has been built.

The general layout of the Crystal Box detector is seen in Fig. 1. A side view of the detector is given in Fig. 2. Photon conversion position information, as well as good electron and photon energy resolution, is achieved by using an array of 396 NaI(Tl) crystals in a configuration that optimizes the detector solid angle for a given cost. Inside the NaI(Tl) array there is a 36-counter hodoscope to identify electrons and provide fast trigger and timing information. The cylindrical drift-chamber fits inside the hodoscope. It provides trajectory information on charged particles and is used to determine origins of decay electrons. A thin (330-μm) polystyrene target with a 50-mm radius is located at the center of the drift-chamber for stopping muons at instantaneous rates of 10^7/sec.

2. Drift-chamber design

The chamber has 728 drift cells arranged on 8 concentric layers with radii between 105 and 220 mm. The wires of each layer are at alternating angles of 10° to 16° from the axis of the drift-chamber. This provides 20° to 32° of stereo angle between the cells of one layer and the next. Relevant data for the 8 layers is listed in Table I. Each cell consists of a sense-wire surrounded by 8 field wires. The sense-wires are 25-μm gold-plated tungsten while the field wires are 152-μm gold-plated copper-beryllium. Individual cells on the same layer are separated by guard wires that are held at 90% of the voltage of the cell corner wires. Cells are separated from adjacent layers by guard wires which are held at 72% of the corner wire voltage. This provides an island of relative positive charge that isolates the cells from the region between the layers. These voltage ratios were chosen to keep the field lines as radial as possible so that the drift time is a function only of a track's distance from a sense-wire.

The body of the drift-chamber can be seen in Fig. 3. It consists of 2 endplates held in place by 4 graphite composite tubular columns (25.4-mm diam Graftex) and corner panels of a honeycomb material (6.35-mm thick Hexcell cut from a 254-mm diam tube) to provide torsional support. The graphite columns and the honeycomb panels are attached to the endplates using a structural adhesive (3M type 2216 B/A), separating them by 635 mm.

The endplates[3] are made of aluminum. They are $(470\ mm)^2$ by 35 mm with 150-mm diam holes, located in the center of the endplates, to provide beam entrance and exit ports and access to the target. Each endplate has 4368 holes for the wire feedthroughs which were drilled at compound angles. The holes are located to a precision of 50 μm and their diameters are accurate to 5 μm. These holes are arranged in 24 concentric rings to form the 8 layers of drift cells.

The chamber has an inner and outer window that surround the drift region. The inner window was made from a 127-μm aluminum-coated Mylar sheet formed into a tube with an epoxy seal along the seam. A gas seal is made at the endplate ports using an O-ring and an expansion clamp. There are eight 152-μm plated copper-beryllium wires (tensioned to 10 N) that are parallel to the chamber axis and attach to the inner window expansion clamps. These wires keep the inner window from collapsing due to the pressure of the gas in the chamber. The target support frame is also held in place by wires which attach to the expansion clamps.

The outer window was made of 254-μm aluminum-coated Mylar which was wrapped around the chamber after all the wires had been strung and sealed with epoxy and a clamping band. This window has had its aluminum coating etched away in a repeating pattern of $(6 \times 40)\ mm^2$ slots to provide many small clear "view ports" into the chamber. These view ports may be used to inspect the drift-chamber interior while replacing broken wires.

The aluminized inside surfaces (facing the drift cells) of both the inner and outer windows are set to an appropriate voltage so that the electrical environments of drift-cell layers 1 and 8 match that of layers 2 through 7. The outside surface of each window is held at ground along with the aluminum endplates.

The materials used in the construction of the drift-chamber were chosen to minimize the amount of mass between the target and the NaI(Tl) crystal array. Table II lists the contributions of the individual components to the total 6.73×10^{-3} radiation lengths for the chamber.

3. Construction and operation

The chamber body was assembled in a precision optical alignment station so that tight tolerances could be maintained as the structural adhesive dried. Then it was moved to a clean room where the feedthroughs were installed. Both sense and field wires used the spring-loaded wire feedthrough assembly shown in Fig. 4. The feedthroughs were made of injection-molded nylon.[4] Each feedthrough was cooled in a liquid-nitrogen bath and then quickly placed into a feedthrough hole on the endplate. When the nylon warmed, it expanded so that a gas seal was formed at both the top and bottom of the hole. As the feedthroughs were installed, they were checked at high-voltage by measuring their leakage current.

Stringing of the wires took place in a clean room with the chamber mounted on a stand that allowed it to be tilted and rotated about the vertical. In this way the wire being strung could be aligned vertically and loaded to the appropriate tension by attaching weights to it. The sense-wires were tensioned with 40 g and the field wires were tensioned with 100 g weights. Wires were strung from the smallest diameter ring out to the largest diameter ring and the tension of each wire was checked by measuring its fundamental frequency of vibration before going on to the next ring. Figure 5 shows the drift-chamber after completion of the stringing operation. The sense-wire positions are known to within 90 μm rms.

After all 8 layers were strung, the feedthroughs were sealed using gas caps which were injection-molded out of polyethylene. Caps on the beam downstream end (the end without the springs) also form a gas seal around the copper tubes which project through these caps. Electrical connections for both field and sense-wires were made by placing connector jacks (Cambion PN 450-3367) on the protruding copper tubes at the downstream end of the chamber. Then the outer window was installed and the chamber wired for high-voltage and sense-wire readout. Figure 6 shows the completed drift-chamber. High-voltage connections were made in small groups of 5 cells each so that a defective cell can be disconnected, allowing operation of the remainder of the chamber to continue.

Voltage is supplied to the chamber by a programmable power supply.[5] Each layer has three separate high-voltage channels, one for the corner, the inter-cell, and the inter-layer field wires. A microcomputer[6] is used to continuously monitor the high-voltage power supply, ramp the chamber voltages up or down, and to sound an alarm should any channel trip off due to excessive current. The

power supply has spark-detection circuitry and over-current detection built into each channel. Should a current surge be detected, or the current exceed a programmed value, the affected channel is immediately shut down to avoid driving destructive energy into a malfunctioning cell. The chamber draws about 16 μA per voltage channel when operated at an instantaneous muon stopping rate of 10^7/sec.

The microcomputer also monitors the gas mixture used in the drift-chamber. Gas flows through gas monitoring chambers (GMC's) before entering and after exiting the chamber. These GMC's consist of 3 drift cells strung in a small volume cavity with a Sr^{90} line source illuminating the cells. GMC cells are identical to cells in the drift-chamber except they are only 152 mm in length and are operated at a voltage that makes them 50% efficient. By monitoring singles rates from the GMC's at a set amplifier-discriminator threshold level, variations in the gas gain can be observed. This system is sensitive to a 0.5% change in the drift-chamber gas mixture within 10 minutes of the change. The exit GMC also has a trigger counter mounted opposite the source so that the drift velocity of the gas exiting the chamber can be measured. For the standard gas mix of argon-ethane-isopropyl alcohol in the ratio 49:49:2, the drift velocity obtained (with the chamber 200 volts above the knee of the voltage plateau) was 50.96 ± 0.38 μm/nsec. LAMPF is at an elevation of 2126 m above sea-level so the chamber's pressure was only 77% that of a sea-level chamber operating at atmospheric pressure. Evaluating our drift velocity at the appropriate ratio of electric field to pressure and allowing for a small effect due to the alcohol, our drift velocity is in agreement with Ref. 7.

The gas mixture used gave good gain and drift-time uniformity when tested in the prototype drift-chambers we built. We found that the prototype chambers would not run properly at high rates without alcohol. The glow discharge symptoms seen in prototype chambers were stopped by the addition of 2% alcohol to the gas mix. Isopropyl alcohol was chosen because it is the least corrosive of the commonly used quenching agents. The argon and ethane are mixed using a commercially available system (Air Products gas blender, model no. FMP 350). After mixing, the argon-ethane gas is held in a large-volume tank at a pressure of 1400 to 2100 g/cm^2. This holding tank helps to minimize the effects of small variations in gas mixing caused by temperature changes and flow regulators turning on and off. Alcohol is added by sending the argon-ethane mixture through a gas-washing bubbler located inside a small refrigerator. The amount

of isopropyl alcohol added is controlled by regulating the temperature of the refrigerator. The gas flow rate is 12.5 cc/sec.

Figure 7 shows the scheme of the chamber readout system. Sense wires are coupled to amplifier-discriminators via 7.5 m of RG-188/U coaxial cable. An inexpensive, flexible amplifier-discriminator system that operates efficiently was designed at LAMPF. These amplifier-discriminators are packaged in double-wide NIM modules that contain 32 channels each. Inputs to these modules are through 34-cable connector blocks (Coaxicon). The outputs are ecl-level logic and are through 34-pin connectors designed for flat twisted-pair ribbon cable. The threshold voltage is supplied in common to all 32 channels of each module from a front-panel jack. The chamber threshold is typically set to about 400 μv but can be as low as 150 μv.

The amplifier-discriminator is based on a high-gain video integrated-circuit amplifier and a high speed ecl comparator. The amplifier (NE592) has a DC differential gain of ×168 and a pole at 4 nsec which corresponds to a -3 dB rolloff at approximately 40 MHz. The input circuitry has a string of ferrite beads (to damp high-frequency ringing) and a spark-suppressing pair of diodes. The amplifier drives an RC-differentiator with a 100 nsec time constant. The differentiated signal is connected to a fast comparator (AM685). The threshold control is provided by offsetting the comparator's positive input by the negative front-panel threshold voltage. The comparator generates an ecl-level signal when the threshold voltage is exceeded. It stays latched for 150 nsec after the triggering signal, independent of the state of the input. Tests performed on a prototype chamber demonstrated that the resolution was only weakly dependent on the amplifiers' high-frequency response and depends strongly on the low-frequency gain. However, the crosstalk was totally dependent on the high-frequency part of the sense-wire signal. Reducing the bandwidth strongly suppressed the cross talk. We were able to achieve individual cell rms spatial resolutions of 110 μm, with inter-cell cross talk at less than 4.2% for the prototype drift-chamber.

A LeCroy 4290 drift-chamber TDC system is used for chamber readout. This system consists of LRS-4291B TDC modules which are housed in a dedicated CAMAC crate with an LRS-4298 controller module in the controller position. This crate controller acts as a fast readout pre-processor, rejecting zero- or full-scale values returned by the 728 TDC's. Valid data are transfered via a 50-pin flat ribbon cable to the LRS-4299 Databus Interface module which is read by the

experimental computer (a PDP 11/44). The TDC's are run in the common-stop mode and set to 512 nsec full scale with 1.0-nsec resolution. The common-stop mode allows a fast inhibit signal which eliminates problems due to multiple pulsing. This system also allows automatic correction of pedestal and gain variations. Zero-channel information is obtained for each of the 728 drift cells by applying a test pulse to the sense-wires at the chamber.

4. Results

The voltage plateau curve for the chamber is shown in Fig. 8. This curve was obtained using decay electrons that triggered an element of the 36-counter hodoscope surrounding the chamber. The nominal operating voltage for the chamber is 2500 volts, 200 volts above the knee of the voltage plateau curve. A typical reconstructed track is shown in Fig. 9.

The observed efficiencies of the individual layers are greater than 99% at low rates. This efficiency goes to 97% at instantaneous muon stopping rates of 10^7/sec. A layer is defined to be efficient if there is a hit on that layer within 5 mm of a track defined by the other 7 layers.

At present we have achieved position resolutions for the 8 layers of 280 to 350 μm and are able to reconstruct 86% of the tracks. The chamber resolution can be improved by including TDC zero-channel information, the known positions of the wires, and an electron-energy cut in the track-fitting algorithm.

Since all the layers are at stereo angles the track-reconstruction algorithm requires hits on at least 6 of the 8 layers in order to solve the ambiguity problem. The ratio of tracks with 6,7, or 8 layers used by the track-fitting algorithm is 2:3:5. The fitting algorithm choses between 16 of a possible 256 ambiguity cases on the bases of χ^2. The χ^2 distribution shows long tails due to multiple scattering. The reconstruction program can solve a simple track in about 1 sec on a PDP 11/44 or in 0.2 sec on a VAX 11-780. The track-fitting algorithm is so slow because the full three dimensional problem of 4 unknowns must be solved, a result of having no wires parallel to the chamber axis.

5. Acknowledgments

We would like to thank the technicians at LAMPF for their tremendous effort in completing the chamber in time for the November 1982 run. In particular we are indebted to J. Conway, C. Espinoza, J. Harshman, B. Martinez, and D. Sanchez

for their careful stringing of the chamber, and also A. Harvier and J. Sandoval for their extensive work on the amplifier-discriminator modules and the readout system. We also wish to thank the rest of the Crystal Box collaboration for their many contributions.

References

1. R. D. Bolton, R. D. Carlini, M. D. Cooper, Minh Duong-Van, J. S. Frank, H. S. Matis, R. E. Mischke, V. D. Sandberg, J. P. Sandoval, R. L. Talaga, Nucl. Instr. and Meth. 188 (1981) 275.

2. Minh Duong-Van, C. M. Hoffman, H. S. Matis, and J. D. Bowman, LAMPF Proposals Nos. 400 and 445, unpublished.

3. Endplates machined by Nu Con Corperation, Livonia, Mich., USA.

4. Feedthrough assembly pieces supplied by Hartzell Custom Products, Turtle Lake, Wis., USA.

5. B-Hive system with 16, B7.5N dual power supplies by Bertan Associates, Inc., Syosset, NY, USA.

6. HP-85 microcomputer by Hewlett-Packard Co., Corvallis, Or., USA.

7. Y. Chatelus, P. Ramanantsizehena, J. Gresser, and G. Schultz, Nucl. Instr. and Meth. 171 (1980) 127; B. Jean-Marie, V. Lepeltier and D. L'Hote, Nucl. Instr. and Meth. 159 (1979) 213.

Figure Captions

Fig. 1 General layout of the Crystal Box detector.

Fig. 2 Side view of the Crystal Box detector.

Fig. 3 Drift-chamber body. The chamber is seen here with all 8736 feedthroughs installed. The feedthroughs are color coded: red for corner field wires, green for inter-cell field wires, blue for inter-layer field wires, and black for the sense-wires.

Fig. 4 Feedthrough assembly. Wires are secured in the copper tubes by a crimp which also provides a shoulder for the tensioning spring on the beam upstream feedthrough (a). On the downstream feedthrough (b), the copper tubes protrude through the gas-sealing cap so an electrical connection can be made.

Fig. 5 Drift-chamber with all wires strung. The chamber is seen here mounted on its assembly stand at the completion of the stringing operation.

Fig. 6 Completed drift-chamber. The finished drift-chamber is seen here in preparation for bench tests with cosmic rays. Assembling the chamber took 4000 man hours.

Fig. 7 Schematic diagram of the drift-chamber readout system.

Fig. 8 Voltage plateau curve. The efficiency shown is not corrected for readout electronics inefficiencies.

Fig. 9 A typical track-reconstruction for a 1e trigger event is shown in several projections.

TABLE 1: Data on the cell layers (at the endplates).

Layer number	No of drift cells	Radius (mm)	Stereo angle (deg)
1	56	105.26	-10.00
2	66	121.31	+10.81
3	76	137.53	-11.65
4	86	153.90	+12.50
5	96	170.36	-13.35
6	106	186.87	+14.20
7	116	203.42	-15.06
8	126	220.01	+15.91
Total =	728		

TABLE II: Drift-chamber mass data.

Material	Thickness (cm)	Density (g/cm^3)	Radiation Length (g/cm^2)	Contribution ($\times 10^{-4}$ rad. lengths)
Mylar	0.0381	1.39	39.95	13.26
Argon	5.75	0.00178	19.55	5.24
Ethane	5.75	0.00136	45.0	1.73
Copper-beryllium	0.0073	8.23	12.86	46.93
Tungsten	0.0004	19.3	6.76	0.12
			Total = 6.73×10^{-3}	

Fig. 1 General layout of the Crystal Box detector.

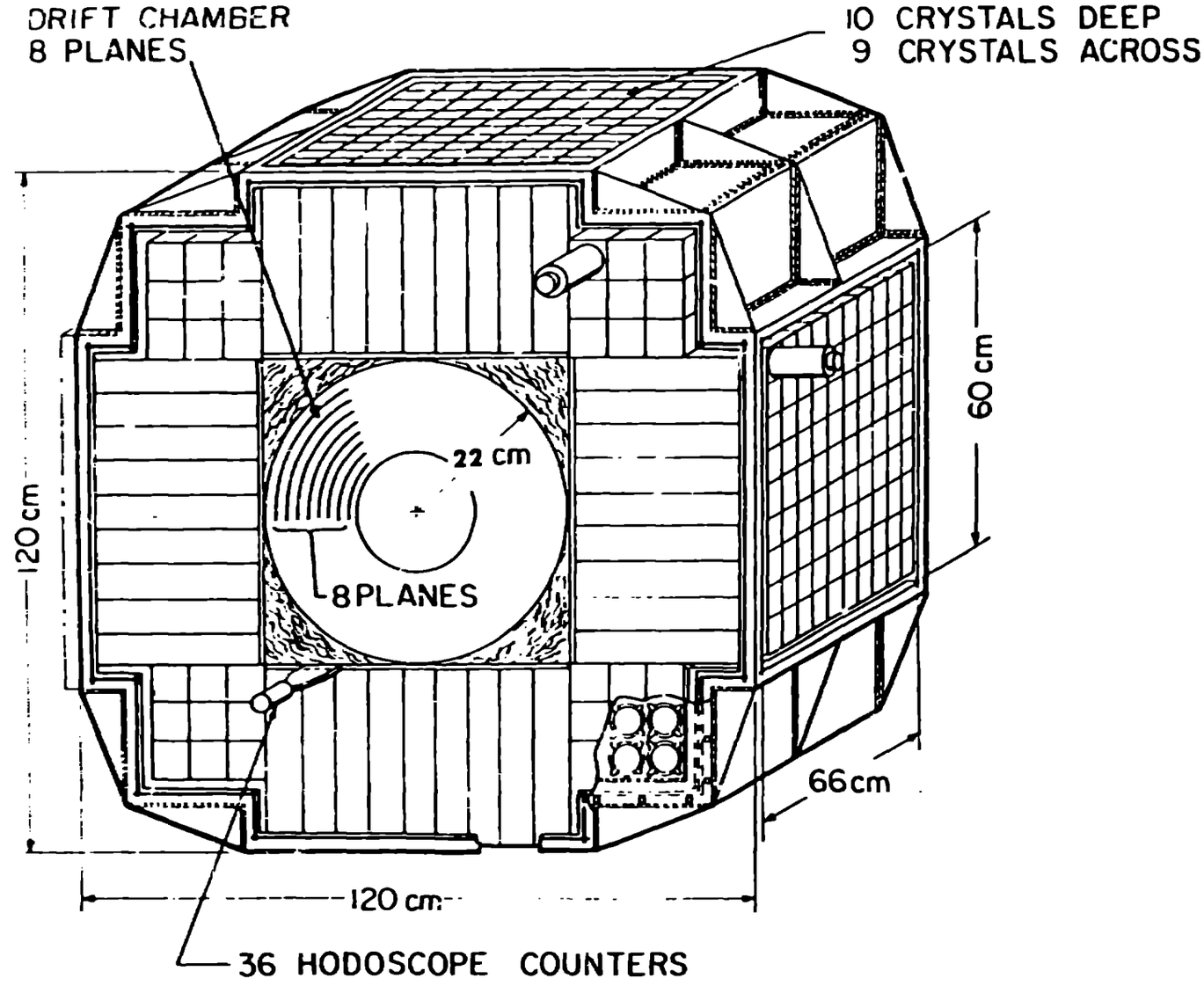

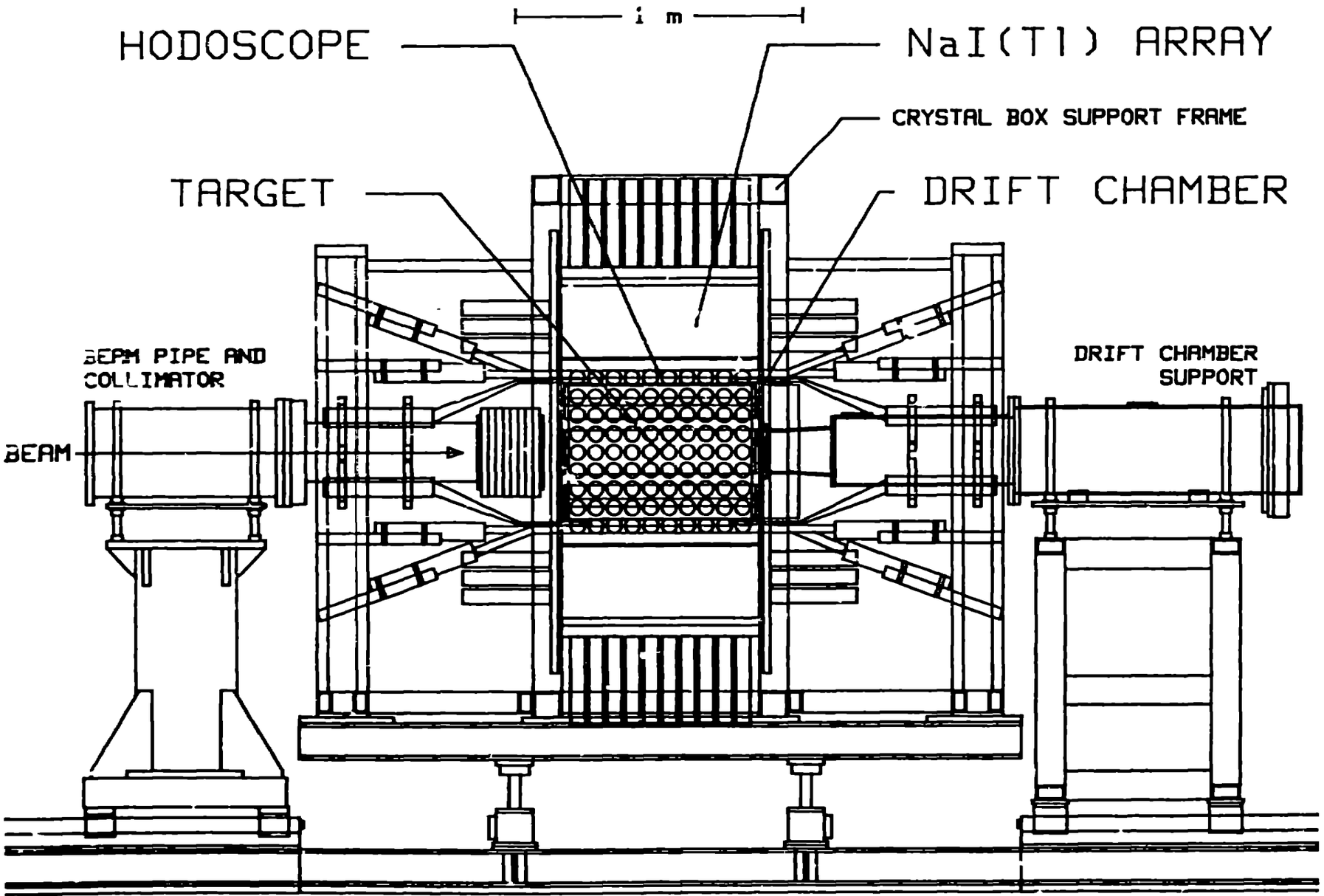

Fig.2 Side view of the Crystal Box detector.

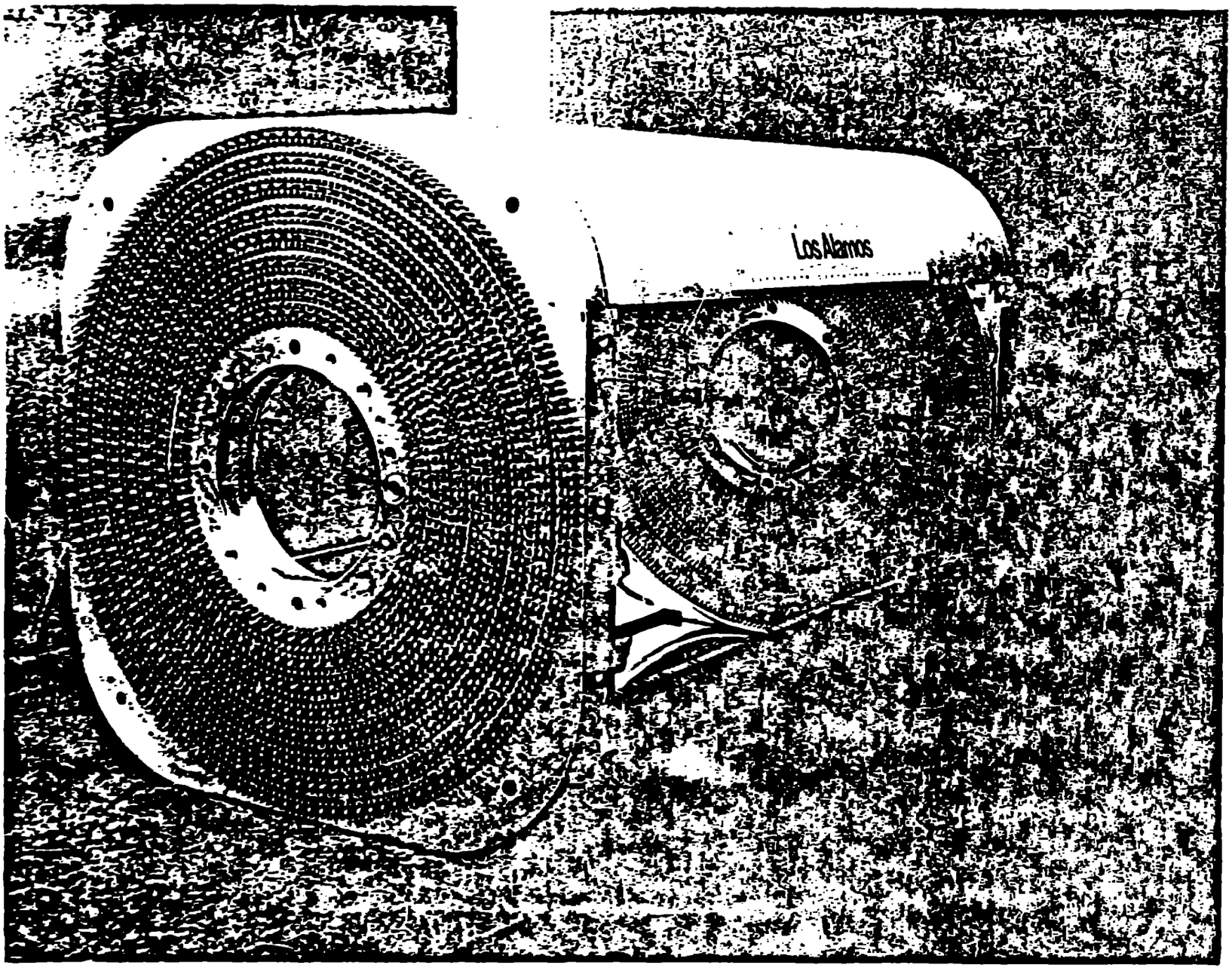

Fig. 3 Drift chamber body.

(a) UPSTREAM FEEDTHROUGH.

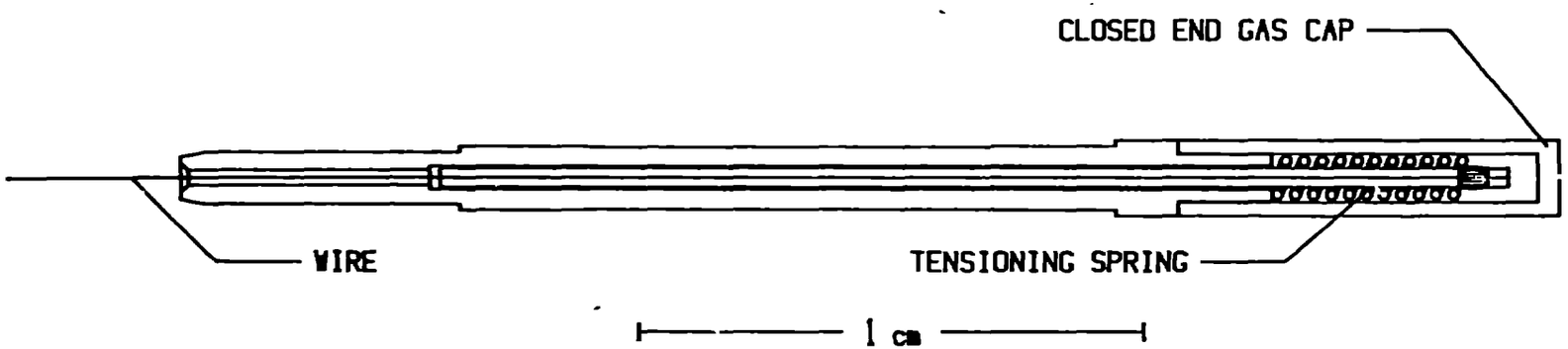

(b) DOWNSTREAM FEEDTHROUGH.

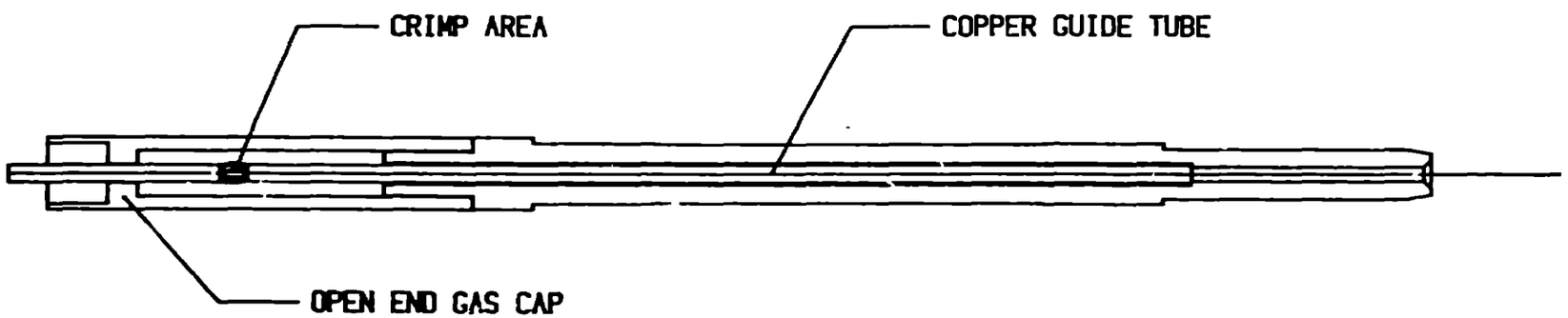

Fig. 4 Wire feedthrough assembly.

Fig. 5 Drift chamber with all wires strung.

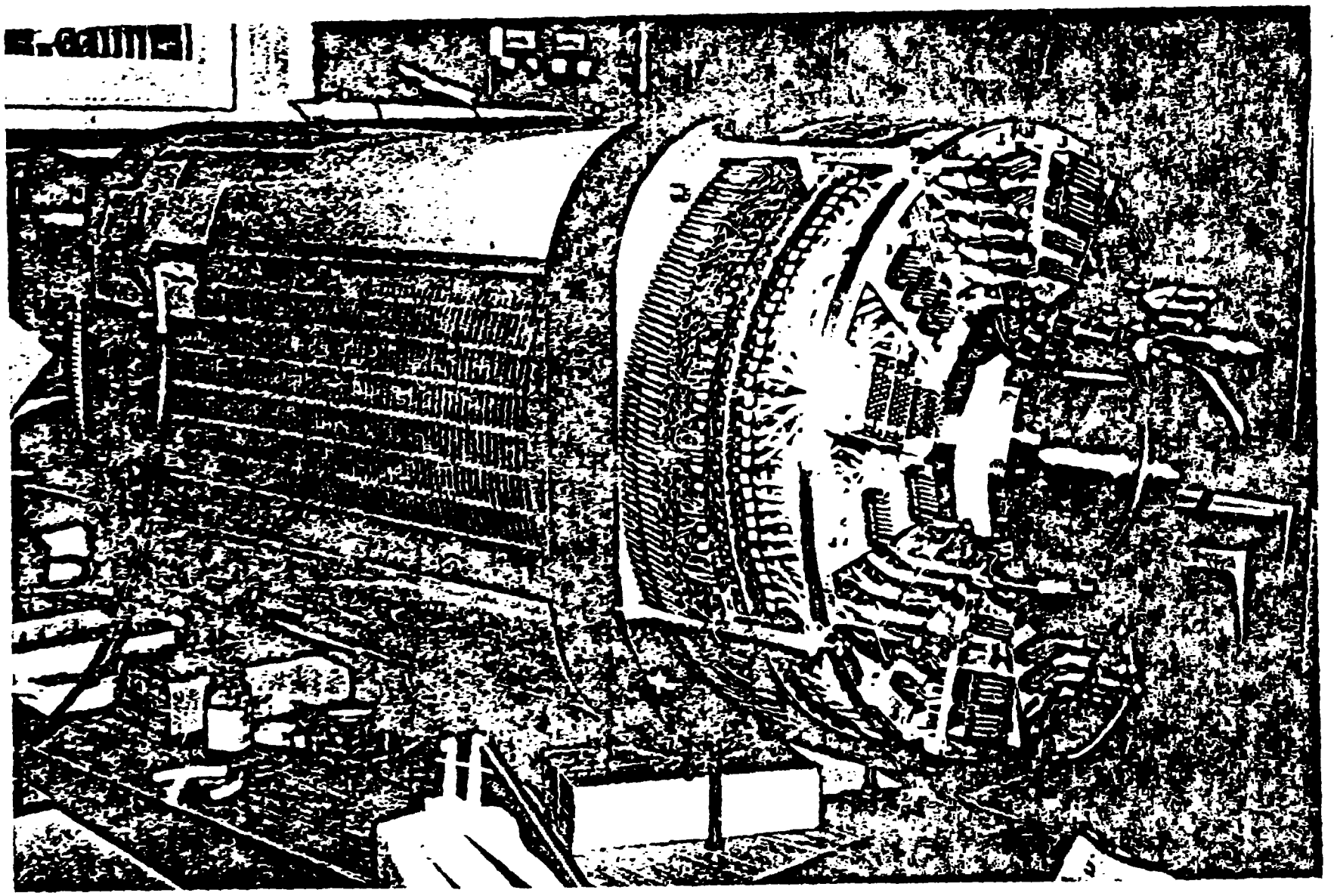

Fig. 6 Compieted drift chamber.

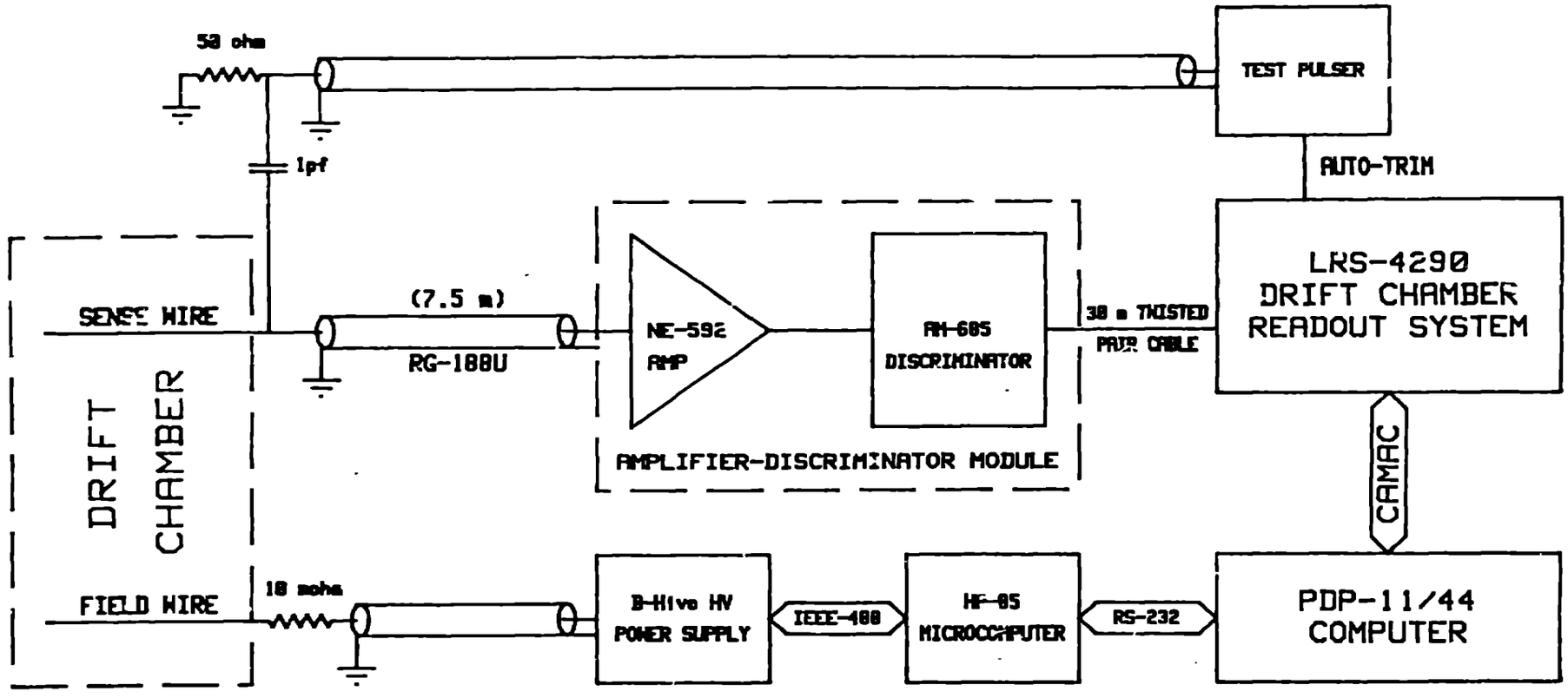

Fig. 7 Schematic diagram of the drift chamber readout system.

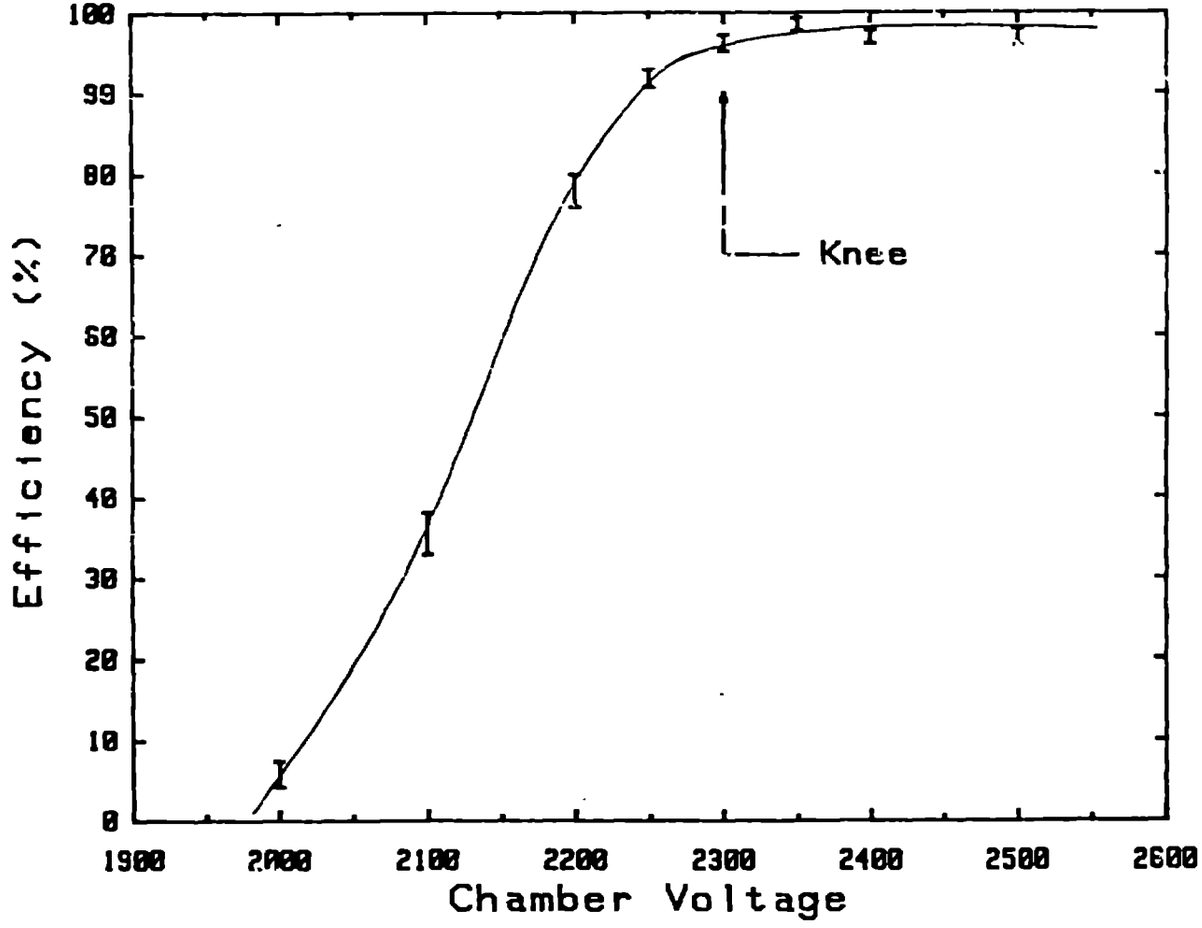

Fig. 8 Voltage plateau curve.

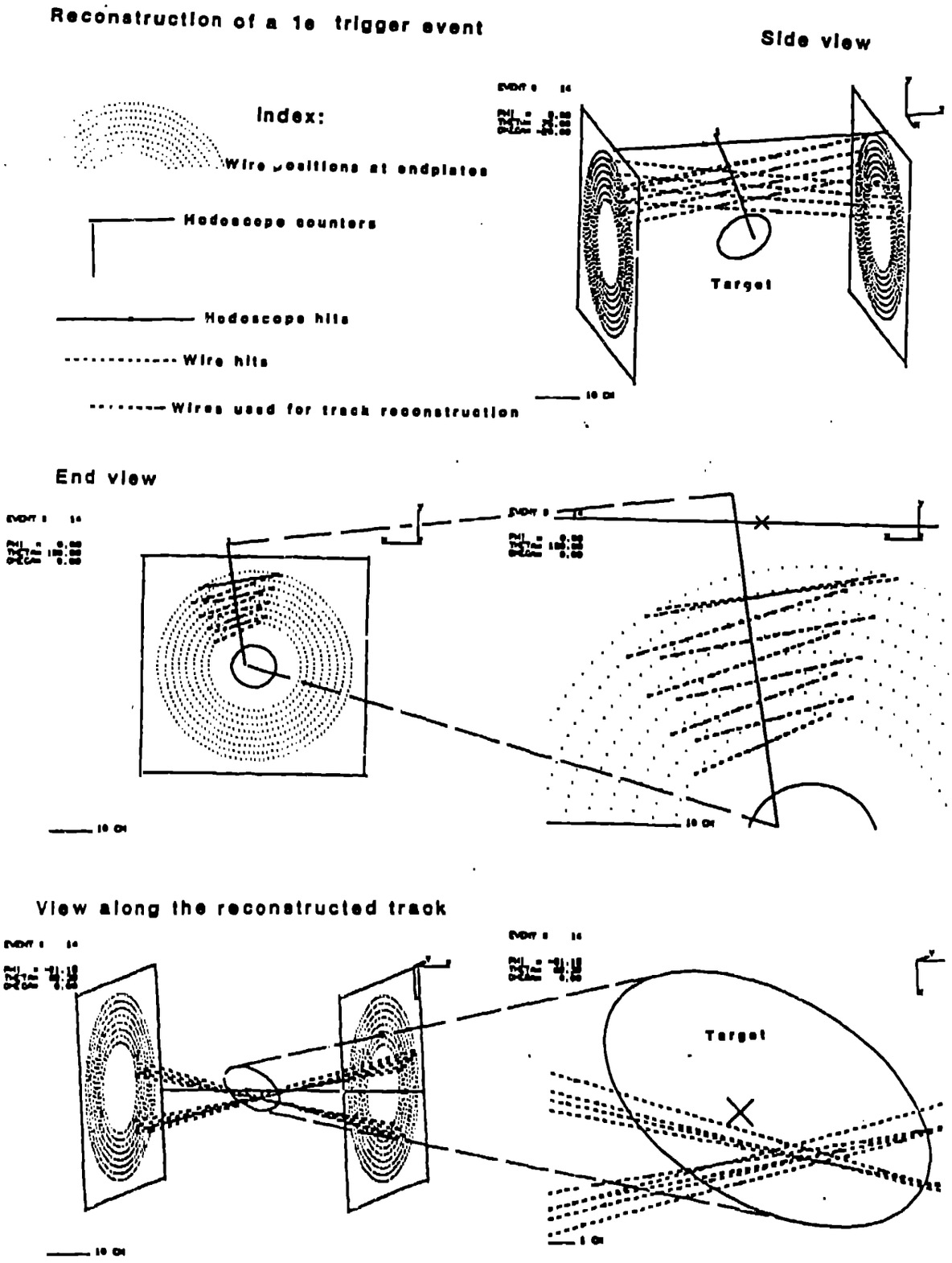

Fig. 9 A typical decay electron event.